THE ASTROPHYSICAL JOURNAL, 425:802–813, 1994 April 20

RAPID COOLING AND THE STRUCTURE OF NEUTRON STARS

JAMES M. LATTIMER
Department of Earth and Space Sciences, State University of New York at Stony Brook, Stony Brook, NY 11794
KENNETH A. VAN RIPER
Radiation Transport Group, Applied Theoretical Physics Division, Los Alamos National Laboratory, Los Alamos, NM 87545
AND
MADAPPA PRAKASH AND MANJU PRAKASH
Department of Physics, State University of New York at Stony Brook, Stony Brook, NY 11794
Received 1993 July 30; accepted 1993 October 28

ABSTRACT

Recently proposed neutrino emission processes in high-density matter result in the relatively rapid cooling of a neutron star's interior followed by a precipitous drop in the surface temperature. We show that the time interval between the formation of the neutron star and the drop in the surface temperature is primarily determined by the structure of the neutron star and is relatively insensitive to the rapid cooling mechanism itself. Thus, observations of thermal emissions from neutron stars have the potential for constraining the neutron star's structure and the underlying equation of state of dense matter.

Subject headings: dense matter — stars: evolution — stars: interiors — stars: neutron

1. INTRODUCTION

Although the masses of several neutron stars have been reliably determined, the structure and interior constitution of neutron stars remain elusive. Theoretical estimates of a neutron star's radius are in the range 8–20 km, which indicates the present uncertainty in the supranuclear equation of state (EOS). Direct observational determinations of a neutron star's radius, from cyclotron line features in the spectra of X-ray pulsars (Hoshi 1992), from X-ray bursts (Inoue 1992), and from the SN 1987A neutrinos (Lattimer & Yahil 1989), for example, are not currently very accurate. However, as we show in this paper, the detection of true thermal emission from a neutron star has the potential of establishing a neutron star's structure, and, by inference, could constrain the EOS of dense matter.

Neutron stars are born with interior temperatures of order 20–50 MeV, but cool via neutrino emission to temperatures of less than 1 MeV within minutes (Burrows & Lattimer 1986). The subsequent cooling consists of two phases: a neutrino-dominated cooling epoch followed by a photon-dominated cooling epoch. Even during the neutrino epoch, thermal photons are radiated from the neutron star's surface. The temperature and luminosity of this thermal radiation is controlled by the interior temperature evolution of the star. Until recently, the general view was that the interiors of newly-formed neutron stars would cool relatively slowly, unless they contained nonstandard or exotic matter, such as a pion condensate, a kaon condensate, or quark matter. In the standard model, the interior cooling is slow enough that the surface temperatures of neutron stars remain above 10^6 K for about 10^5 yr, and they are potentially observable for this length of time in the X-ray or UV bands. When exotic matter with enhanced neutrino emissivity is present, the core cools so rapidly that a temperature inversion develops. The size of the cooler interior grows as the energy from the hot crust is conducted to the core. After about 1 to 100 yr, depending upon the star's structure, this cooling wave reaches the surface and the surface temperature plummets, perhaps to unobservably low values.

However, Lattimer et al. (1991) and Prakash et al. (1992) have suggested the possibility that all neutron stars will cool rapidly, whether they contain exotic matter or not. Lattimer et al. (1991) showed that ordinary (nonexotic) matter with a proton/nucleon ratio in excess of some critical value lying in the range 0.11–0.15 can cool by the direct Urca process even more rapidly than matter in an exotic state. Prakash et al. (1992) further showed that matter with *any* proton/nucleon ratio can rapidly cool by the direct Urca process if Λ hyperons are present. In addition, in the presence of a pion or kaon condensate, Thorssen, Prakash, & Lattimer (1994) have shown that the proton fraction will necessarily rise to values in excess of the Urca threshold. It is not unlikely that one or more of these situations will, in fact, occur in neutron stars.

The time for a neutron star's center to cool by the direct Urca process to a temperature T has been estimated to be about

$$t = 20 T_9^{-4} \text{ s} \quad (1)$$

(Lattimer et al. 1991), where $T_9 = T/10^9$ K. The direct Urca process and all the exotic cooling mechanisms only occur at supranuclear densities. Matter at subnuclear densities in the neutron star's crust cools primarily by diffusion of heat to the interior. Thus, the surface temperature remains high, in the vicinity of 10^6 K or more, until the crust's heat reservoir is consumed. After this diffusion time, which is of order 1–100 yr, the surface temperature abruptly plunges to values below 5×10^5 K. The diffusion time depends upon the size of the crust, the heat capacity, and the thermal conductivity of the matter at subnuclear densities. It does not, as we will demonstrate, depend upon the details of the core cooling mechanism, assuming, of course, that sufficiently rapid cooling occurs at all. The direct Urca process is estimated to occur for densities in excess of 2–3 times the standard nuclear density, $\rho_0 = 2.7$

$\times 10^{14}$ g cm^{-3}, and is faster than the conventional cooling mechanism, the modified Urca process, by a large factor of about $5 \times 10^5 T_9^{-2}$. Since core temperatures become less than $T_9 = 1$ after several seconds, this cooling mechanism is sufficiently rapid.

The extent to which the surface temperature finally drops is chiefly determined by the core temperature. If the direct Urca process in the core continues unabated, the core temperature as a function of time is given by inverting equation (1), or

$$T_{\rm core} \sim 3 \times 10^7 (t/{\rm yr})^{-1/4} \ {\rm K} \ . \qquad (2)$$

The surface temperature will be about a factor of 100 less than this, depending on the details of the star's envelope (Van Riper 1988). However, when the core temperature drops to 1 MeV or less, nucleons in the neutron star's core may become superfluid. If this happens, the neutrino emissivity from the direct Urca process will be quenched by a factor $\approx \exp(-\Delta/kT)$, since, for the process to occur, the total energy of particles in the initial or final state must exceed Δ, the larger of the neutron and proton gaps. The size of the gaps are uncertain but have been calculated to be on the order of a few hundred keV. Thus, when $kT \ll \Delta$, the neutrino cooling is significantly reduced. As Page & Applegate (1992) have shown, nucleon superfluidity results in surface temperatures that are intermediate between those produced by standard cooling and unquenched rapid cooling. They suggest that observations of neutron stars with these intermediate surface temperatures would be evidence of nucleon superfluidity. Actually, if a cooling process could be found that was just a few times faster than the modified Urca process, or if the region in which a rapid cooling process occurred was limited to a tiny fraction ($\lesssim 10^{-4}$) of the core, it would also be possible to achieve intermediate temperatures in the absence of superfluidity. However, at present, neither of these situations seem likely.

Nonetheless, it is uncertain that nucleon superfluidity persists to the highest densities found in the centers of neutron stars. Moreover, it is likely that hyperons are present at supranuclear densities. Nucleon superfluidity would not necessarily quench the hyperon Urca process and it is not known if hyperons themselves form superfluids in neutron stars. As long as there exists a core or region in which an unquenched Urca process can operate, the surface temperature would fall to unobservably low values. Even potential heating processes, such as those due to friction between the rotating superfluid and normal parts of the star, or to the decay of the magnetic field, would not be strong enough to prevent the surface temperatures from dropping precipitously.

Nearly all potential candidates for thermal emission (see, e.g., Tsuruta 1986; Ögelman 1993; Becker, Trümper, & Ögelman 1993) are pulsars, and it is unclear how much of the observed emission is due to the pulsar phenomenon, to a synchrotron-emitting nebula, or to thermal emission from the neutron star itself. Improved spectral resolution in recent observations shows strong evidence for a thermal spectrum in sources such as PSR 0656+14 (Córdova et al. 1989), PSR 1055−52 (Brinkmann & Ögelman 1987) and Geminga (Halpern & Holt 1992). Periodicity in the thermal emission from PSR 0656+14 is interpreted as a hotter region on the surface sweeping past the field of view as the star rotates (Finley, Ögelman, & Kızıloğlu 1992; Anderson et al. 1993). All objects observed to date, with the exception of SN 1987A, are more than 100 yr old, and the rapid cooling paradigm suggests that no thermal emission will be observed from them. In the case of SN 1987A, no thermal emission is seen as yet. Rapid cooling may be the reason for the absence of thermal emission from the young neutron stars which may be present in the center of the Kepler (Helfand, Chanan, & Novick 1980), Tycho (Gorenstein, Seward, & Tucker 1983), or SN 1006 (Pye et al. 1981) supernova remnants.

In this paper we show that there is a straightforward relationship between the diffusion time and the thickness of the crust of a neutron star. We will define precisely what we mean by the crust in § 2. Such a result has been anticipated by Brown et al. (1988), who argued that the time needed for a temperature drop in the inner core to significantly affect the surface temperature was about $R_{\rm shell}^2/D$, where $R_{\rm shell}$ is the thickness of a neutron star's crust and D is the diffusivity of the crust. By including general relativity and making use of detailed numerical models, we will make this relationship quantitatively useful. Thus, the crust thickness, the neutron star's mass and radius, and the EOS are intimately related. Therefore, should the surface temperature plunge ever be observed, the mass and radius of the neutron star could be constrained. Coupled with other observations, it is possible that properties of the supranuclear EOS could be estimated.

In § 2, results of full numerical simulations of cooling neutron stars, covering a variety of cooling mechanisms, EOSs, superfluid models, and neutron star masses are given. In § 3, the diffusion of heat from the crust of a neutron star is treated with analytical models. These models establish general numerical relations between the neutron star's structure and the diffusion time. These results are compared to the numerical simulations, which can be used to calibrate the analytic models. In § 4, the relationships between the crust thickness, the neutron star mass and radius, and the EOS are detailed, and the prospects of using observations of thermal evolution to constrain neutron star or nuclear matter properties are discussed.

2. NUMERICAL SIMULATIONS

2.1. *Cooling Model*

Figure 1 illustrates schematically the essential structure of a neutron star which is relevant for cooling simulations. First, there is a core, of radius $R_{\rm core}$, in which the density exceeds the value $\rho_{\rm core}$, which is of order ρ_0. In the event of rapid cooling, the core cools much more quickly than the crust (see eq. [1]) and, because the thermal conductivity is high above nuclear density, reaches isothermality in a few hours. The core is surrounded by a crust which acts as a heat reservoir. We are basically interested in the diffusion of heat through the crust, which has a thickness ranging from 0.4–3 km, depending on the EOS and the neutron star's mass. We will define the crust, whose width is $R_{\rm shell}$, to be the region bounded on the inside by the density $\rho_{\rm core}$. This is not necessarily the same definition used, for example, in theories of glitches, in which the crust refers to the region in which nuclei coexist with (partially superfluid) neutrons. The "glitch crust" has an inner boundary defined by the density at which nuclei merge into a uniform nuclear sea of neutrons and protons, which occurs at densities perhaps as low as $\frac{1}{2}\rho_0$ (see, e.g., Lorenz, Ravenhall & Pethick 1993). The actual definition of the crust boundary will not be essential to our conclusions, so long as one is consistent in its definition. We will show in § 4 that the value of $R_{\rm shell}$, for a star of given total mass and radius, depends entirely on the EOS below $\rho_{\rm core}$, which is thought to be relatively well understood.

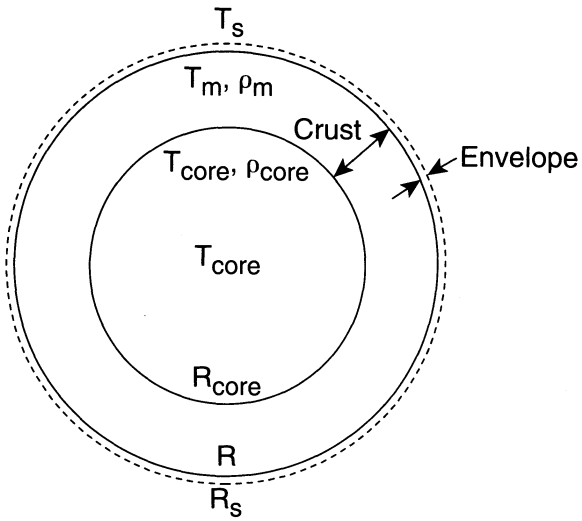

FIG. 1.—Schematic neutron star model. Subscript s refers to the visible surface and is denoted by the dashed circle. The crust-envelope (R, T_m, ρ_m) and core-crust interfaces (subscript "core") are indicated by the solid curves.

Therefore, R_{shell}, defined with a boundary at ρ_{core}, is related by a constant factor (independent of the high-density EOS, the total mass, and the total radius) to the crust thickness defined with another boundary density.

Lastly, an envelope extends from $\rho_m = 10^{10}$ g cm^{-3} to the surface (subscript s). The heat capacity of the envelope, which is very thin in comparison to the sizes of the other regions, is negligible; the surface temperature responds nearly instantaneously to variations in T_m, the temperature at ρ_m. The two boundaries of interest to us are the core-crust interface and the crust-envelope interface. We will calculate the temperature evolution at the crust-envelope interface, given the temperature as a function of time at the core-crust interface. The temperature at the crust-envelope interface is simply related to the visible surface temperature (Van Riper 1988).

We explore the thermal evolution of neutron stars using the general relativistic code developed by Van Riper (1988, 1991). This code uses a diffusion algorithm to follow both the conduction of heat and energy losses by neutrino emission inside the star. Van Riper (1991) has detailed the thermal conductivities, neutrino emissivities, and heat capacities used in this code (see also the next section). We compute the temperature distribution interior to the density 10^{10} g cm^{-3} and treat the envelope external to this as a boundary condition using the algorithm of Van Riper (1988). For all models, a surface magnetic field strength $B = 10^{12}$ G is assumed. Magnetic field effects are important only at densities $< 10^{10}$ g cm^{-3} and can affect the relation between the visible surface temperature and the crust-envelope interface temperature. At higher densities, a field $B \leq 10^{13}$ G has little impact on the conductivity, heat capacity, and EOS and thus will not affect the details of the thermal evolution. Our spherical envelope model is based upon opacities parallel to the field, the direction in which they are most diminished from their nonmagnetic values. Envelope models for other orientations show the parallel envelope results are still appropriate for most of the surface (Miralles & Van Riper 1993). We considered a series of models to explore the dependence of the thermal evolution upon stellar properties, the nature of the cooling process, and the presence and properties of nucleon superfluids, both in the crust and the core.

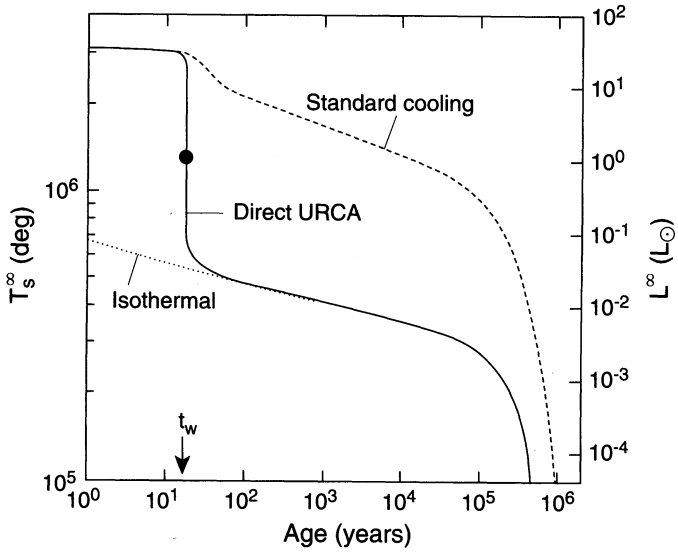

FIG. 2.—Cooling of a neutron star in the standard model compared to the rapid cooling case. In the rapid cooling case, the time necessary for the cooling wave to reach the surface is denoted by t_w. The dotted curve assumes no diffusion and that the core and crust are isothermal.

A typical example of the effect of rapid cooling compared to standard cooling is shown in Figure 2. Here the standard and rapid cooling curves coincide until a cooling wave reaches the surface at $t_w = 15$ yr. We define the cooling time t_w as the instant when the cooling curve has the greatest (negative) slope (indicated in Fig. 2 by the filled circle). Following the abrupt drop in surface temperature, the part of the star interior to the envelope becomes isothermal, as shown in Figure 3. Figure 3 shows how the temperature profiles in the outer parts of a neutron star evolve. Note that the ratio of the temperatures of the crust-envelope interface (T_m) and the core-crust interface (T_{core}) remain uniformly large even as the core is rapidly cooled.

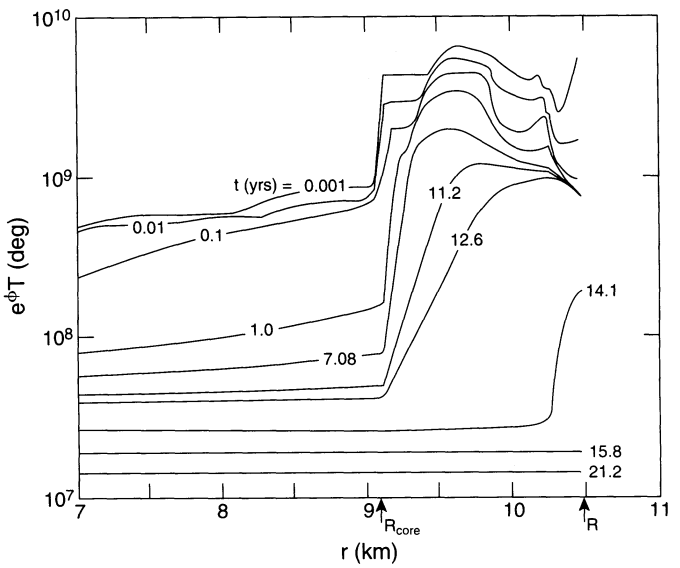

FIG. 3.—Thermal evolution of the outer parts of a neutron star. The redshift is denoted by e^ϕ. Each curve corresponds to the labeled age. The core-crust interface is indicated by R_{core}; curves end at the surface, R.

The cooling in both the standard and rapid cooling cases is dominated by neutrinos until about 10^5 yr when surface thermal photon emission takes over and the cooling curves steepen.

The two most important features evident from Figure 2 are the cooling time t_w and the temperature during the isothermal era. We will delineate how these potential observable parameters could be connected to the EOS or to the structure of the neutron star.

2.2. *Stellar Size*

Our first investigation centers on the dependence of t_w with the size of the star. To facilitate this study, we used the emissivity from the Urca process on percolating quarks (Kiguchi & Sato 1981) for an accelerated cooling mechanism. This particular process has a lower threshold density (equal to nuclear density) than other cooling mechanisms and thus permits accelerated cooling models over a wider range of stellar masses and radii. We effectively varied the stellar radius R by fixing the (gravitational) mass and using different dense matter EOSs or by varying the central density (and hence the mass) while employing a single EOS. For these simulations a variety of EOSs were used. They included those of Prakash, Ainsworth, & Lattimer (1988, hereafter PAL), Friedman & Pandharipande (1981), Pandharipande & Smith (1975), and Baym, Pethick, & Sutherland (1971).

The results are shown in Figure 4, in which t_w is plotted against R. It is evident that a monotonic correlation exists between t_w and R, with t_w roughly varying as R^6. However, the relationship appears to depend on the neutron star mass as well as the radius. The curve obtained by varying the neutron star mass with a fixed EOS has significantly more curvature than do the curves obtained with constant mass.

As we will show in the analytical treatment of § 3, there are strong physical reasons for believing that t_w depends more directly on the thickness of the neutron star's crust than upon R. For the moment, we define $R_{\rm shell} = R - R_{\rm core}$ to be a fiducial measure of crust thickness, where $R_{\rm core}$ is the radius at which the density is equal to $\rho_{\rm core} = \rho_0$, the standard nuclear matter density. Although the definition of $R_{\rm shell}$ seemingly depends arbitrarily upon our choice of the boundary density (in this case ρ_0), the results we will find are, in fact, insensitive to our choice of $\rho_{\rm core}$. As seen in Figure 4, we find that the variation among the curves, and hence the mass dependence, is greatly reduced when t_w is plotted versus $R_{\rm shell}$ compared to R. A rough power-law fit is $t_w \propto R_{\rm shell}^n$, where $1.7 \leq n \leq 1.8$. This general behavior appears to be valid regardless of whether superfluidity is assumed or not, and whether the variation in $R_{\rm shell}$ is due to variations in the total neutron star mass or due to variations in the nuclear EOS. These results will be interpreted in § 4.

2.3. *Crust Size*

In models where crust neutron superfluidity is present, t_w decreases by about a factor of 3 compared to the corresponding nonsuperfluid model. This change is due to the reduction of the heat capacity of the neutrons in the crust. (The particular model for the quark Urca process which produced the rapid cooling in this series of simulations is itself unaffected by core superfluidity; neither is the heat capacity of the quark core.) We will establish in § 4 that t_w is proportional to the specific heat in the crust. Once the neutron contribution to the specific heat is suppressed by superfluidity, the specific heat becomes dominated by the electrons. The effective reduction in the crustal heat capacity in the superfluid case is a complicated average over density and temperature distributions, and we have not found a simple (analytic) explanation for the particular factor of 3 found in our numerical simulations.

2.4. *Cooling Rate*

The next series of numerical simulations focuses on the sensitivity of the thermal evolution to the exact form of the

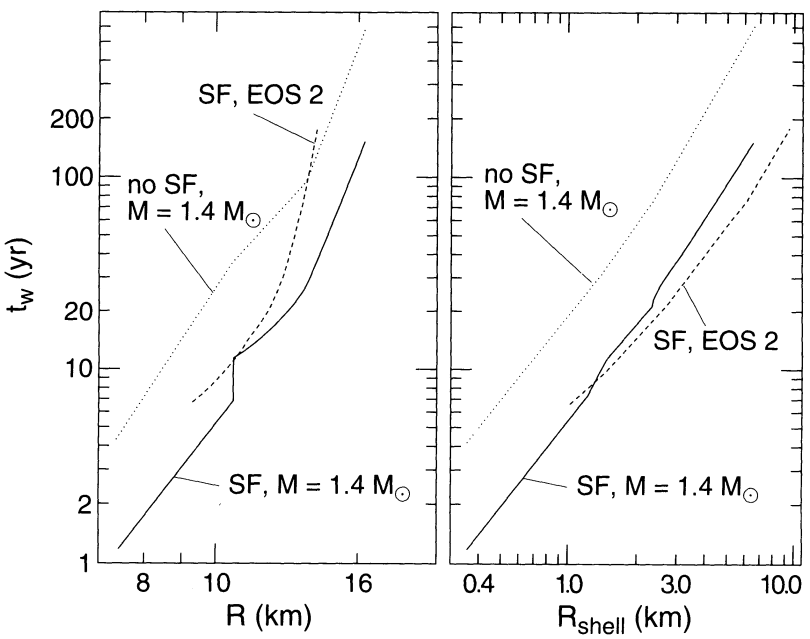

FIG. 4.—Cooling time as functions of neutron star radius (*left*) and neutron star crust thickness (*right*). Cooling by means of the Urca process on percolating quarks is assumed; cases in which nucleon superfluidity exists in the crust are denoted by SF. The solid curves refer to simulations in which the total neutron star mass is fixed at 1.4 $M_\odot$; different neutron star radii and crustal thicknesses are obtained by varying the nuclear EOS. For this figure, $R_{\rm shell}$ is defined by the boundary $\rho_{\rm core} = \rho_0$. The dashed curves show cases in which the EOS was kept fixed and the neutron star mass was varied. See Table 3 for a description of EOS 2.

accelerated cooling process. The processes investigated included:

i) the direct Urca process (Lattimer et al. 1991),

$$\epsilon_{DU} = 4.00 \times 10^{27}\left(\frac{Y_e \rho}{\rho_0}\right)^{1/3} m_n^* m_p^* T_9^6 \text{ ergs cm}^{-3}\text{ s}^{-1}\text{ ;}$$

$$\rho > 4.4\rho_0\text{ ,} \quad (3)$$

ii) the Urca process on percolating quarks (Kiguchi & Sato 1981),

$$\epsilon_Q = 1.56 \times 10^{26}\left(\frac{\rho}{3.07\rho_0} - 0.16\right)^{3.2} T_9^6 \text{ ergs cm}^{-3}\text{ s}^{-1}\text{ ;}$$

$$\rho > \rho_0 \quad (4)$$

and iii) neutrino emission from a pion condensate (Maxwell et al. 1977),

$$\epsilon_\pi = 3.14 \times 10^{25} m_n^{*2} T_9^6 \text{ ergs cm}^{-3}\text{ s}^{-1}\text{ ; }\rho > 2.0\rho_0\text{ .} \quad (5)$$

In these expressions ϵ is the emissivity, m_n^* and m_p^* are the neutron and proton effective masses in units of the nucleon mass, and Y_e is the electron fraction. This series of simulations was performed for a constant neutron star mass of 1.4 $M_\odot$. Different values of R_{shell} were obtained by varying the EOS. Since we wished to examine the relation between t_w and the cooling rate in a fashion that was independent of structural effects, we did not include in these calculations the variations in the star's structure that would have resulted from the quark-hadron transition (in case ii) or the pion condensate (case iii). In reality, stars with phase transitions to quarks or pion condensates can have radically different structures (i.e., much higher central densities and smaller radii) than "normal" stars. The different structures will have a large impact on the cooling times. The effect of phase transitions is covered in more detail in § 4. To recapitulate, at this point we are strictly interested only in the relation between the neutrino emission rate and the effective surface cooling time.

The result of using these physically motivated forms of rapid cooling is shown in Table 1. The cooling times are remarkably insensitive to the details of the cooling process. There is a slight decrease in t_w for stronger cooling models which results from a larger initial decrease in the central temperature. This behavior is predicted by the analytic calculations presented in § 3. That the direct Urca cooling times in two of the superfluid cases exceed those of the slower quark process can be explained by core superfluidity suppressing the direct Urca rate but not the quark rate. Finally, note that when superfluid effects are included in the model (indicated by "SF" in the second column of Table 1), the cooling time t_w is reduced by a factor 3–4 relative to the cooling time when these effects are ignored (indicated by "N") because of the reduction of heat capacity in the crust.

TABLE 1

COOLING TIMES FOR $M = 1.4\ M_\odot$: PHYSICAL MODELS

R_{shell} (km)	SF	t_w(yr) Q	DU	π
0.36	SF	1.17	...	1.37
1.2	SF	6.99	...	7.53
1.5	SF	11.3	11.1	...
1.5	N	35.9	32.9	...
2.0	SF	16.6	17.8	...
2.0	N	59.5	52.8	...
2.4	SF	21.7	31.2	...
2.4	N	77.3	73.4	...

TABLE 2

COOLING TIMES FOR $M = 1.4\ M_\odot$: GENERIC MODELS

ρ_t (10^{14} g cm^{-3})	$\log_{10} A$	t_w (yr)
2.8	28	29.1
2.8	27	32.2
2.8	26	36.2
2.8	25	41.9
2.8	24	48.8
2.8	23	60.4
2.8	26	36.2
5.6	26	37.5
10.0	26	39.7

We also considered a generic accelerated emissivity,

$$\epsilon_G = AT_9^6\text{ ,} \quad (6)$$

to explore the dependencies on the overall magnitude A and threshold density ρ_t separately. The variations t_w with emissivity model are shown in Table 2 and in Figure 5. The dependence of t_w on the parameters for the generic emissivity is slight as long as the overall rate is much larger than that of standard cooling, for which the effective value of A is around 10^{21}. Although there is an apparent increase in t_w with decreasing A, there is very little change in t_w when ρ_t is varied. This emphasizes that there is no need to relate the inner boundary defining R_{shell} with ρ_t. Only the total amount of cooling, integrated over the core, is relevant. The relationship we have obtained, $t_w \propto R_{shell}^n$, where $n \sim 2$, is therefore independent of the precise definition of R_{shell}.

The temperature evolution of the star following the rapid temperature drop at t_w, when the core and crust of the star are isothermal, is determined by the core's cooling rate. The more rapid the cooling rate, the lower the temperature that is

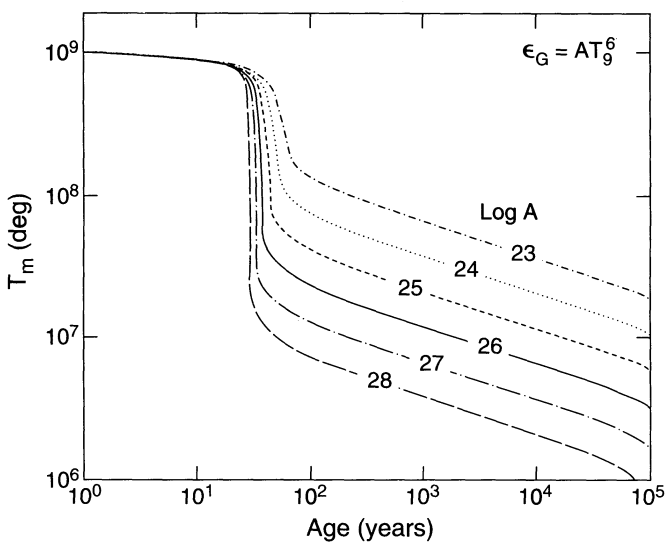

FIG. 5.—Temperature of the crust-envelope interface (T_m) as a function of time for 1.4 $M_\odot$ neutron stars cooling according to eq. (6).

achieved. The temperature during this isothermal epoch can be readily estimated by combining the generic cooling rate, equation (6), with the total heat content of the star. The result is given by a formula analogous to equation (2):

$$T_7 \simeq 2\left(\frac{10^{28}\ \mathrm{yr}}{At}\right)^{1/4},$$

where $T_7 = T/10^7$ K. The calculations in Figure 5 follow this result closely. Surface temperatures that are intermediate between the standard and rapid cooling models can be obtained if the cooling is suitably adjusted. One way of achieving this is to quench rapid cooling with superfluidity, as we now discuss.

2.5. *Crust and Core Superfluidity*

As pointed out by Page & Applegate (1992), when core superfluidity is present, the interior temperature drops to a value determined by the magnitude of the superfluid critical temperature. Page & Applegate argued, further, that the two temperatures are related by $T_{\mathrm{interior}}/T_{\mathrm{crit}} \approx 0.2$. Levenfish & Yakovlev (1992) have shown the suppression of the emissivity is less than assumed by Page & Applegate, so the temperature ratio will be somewhat lower than 0.2. After the cooling wave reaches the surface, the surface temperature reflects the superfluid critical temperature until the onset of the photon cooling epoch. The surface temperature is intermediate between the standard cooling and rapid cooling cases. However, this result only applies to those rapid cooling processes that are quenched by superfluidity. The direct Urca and condensate cooling processes are quenched, but it is uncertain whether quark cooling is also quenched (Bailin & Love 1984). In addition, this result applies only if, effectively, the *entire* core is superfluid. If some part of the rapidly cooling core lies in a density regime outside of the superfluid region, the rapid cooling will continue unabated.

We have considered two models for the superfluid gaps above nuclear density, which are shown in Figure 6. The "standard" model gaps are from Takatsuka (1972) and Chao, Clark, & Yang (1972) for the neutron $^3P_2$ and proton $^1S_0$ gaps, respectively. The extreme model substantially increases both the energy of the gaps and their extent in density. We do not consider the extreme model to be physically realistic, but have included it for the purposes of comparison. The same neutron $^1S_0$ gap of Takatsuka (1972) below nuclear density is used in both cases. This gap does not affect the neutrino emission but is crucial in determining the specific heat of the crust and therefore t_w. In the nonsuperfluid models we omitted both crust and core superfluidity.

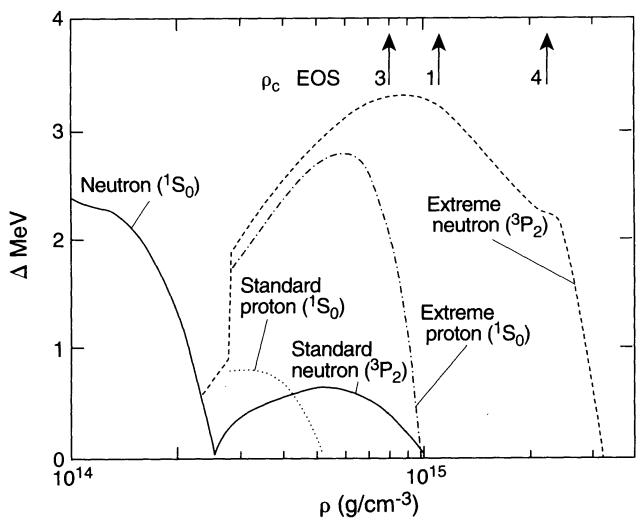

FIG. 6.—Superfluid gaps as a function of density. All superfluid models contain the neutron $^1S_0$ gap which affects the crust. Standard model neutron $^3P_2$ (Takatsuka 1972) and proton $^1S_0$ (Chao, Clark, & Yang 1972) gaps and extreme model gaps are shown. The central density of 1.4 $M_\odot$ stars for the three PAL equations of state are indicated by arrows.

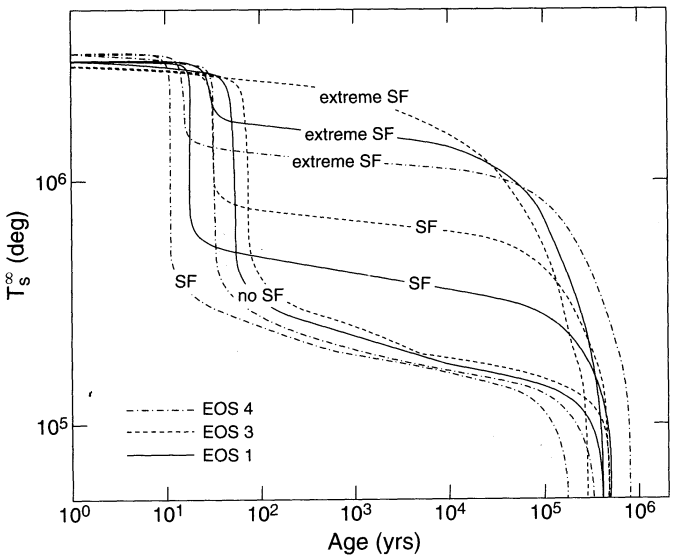

FIG. 7.—Direct Urca cooling of 1.4 $M_\odot$ neutron stars with different treatments of superfluidity. Results for each of three PAL equations of state (see text) for 1.4 $M_\odot$ stars are indicated.

Figure 7 shows the results of cooling simulations using the direct Urca emissivity and different superfluid (SF) gaps for a mass of 1.4 $M_\odot$. The equations of state were taken from PAL and have, as free parameters, the bulk incompressibility (K_0) and the high density stiffness of the EOS (parameterized by the quantity B'). All other EOS parameters are the same as in PAL for the case in which the potential energy contributions to the symmetry energy are assumed to be linear. Positive values of B' yield softer high-density EOSs and smaller values for the maximum mass, relative to the case $B' = 0$. Three different parameter sets were used for these simulations and they are detailed in Table 3. The central densities (ρ_c) of 1.4 $M_\odot$ stars for each of the three parameter sets are also listed in Table 3. With EOS 4, ρ_c is more than twice the highest density of superfluid matter in the standard model, and there is very little difference between the cooling curves with no superfluidity and with the standard superfluidity. There is, however, a difference

TABLE 3

PARAMETERS AND PROPERTIES OF SELECTED PAL EQUATIONS OF STATE

EOS	K_0 (MeV)	B'	$M_{\max}$ ($M_\odot$)	ρ_c/ρ_0 of 1.4 $M_\odot$ Stars
1	180	0.	1.74	3.85
2	180	0.895	1.45	7.77
3	240	0.	2.05	2.81
4	240	0.67	1.44	7.50

in the timing because of the dependence of t_w on the crustal specific heat, which does depend on the existence of superfluidity in the crust. For EOS 1 and EOS 3, the neutron $^3P_2$ gap involves a substantial fraction of the neutrons in the core, and the cooling curves do not drop to as low a level after the time t_w as when the emissivity is not suppressed; the superfluidity effect is greater for lower ρ_c because the effective gap temperature is lower at higher densities. The temperature the core maintains once superfluidity begins is related to an effective critical temperature, as Page & Applegate (1992) found. However, there is no simple relationship between the maximum critical temperature and the surface temperature because of the density dependence of the gap energy. Since the density profile of the core is relatively flat, the effective gap is mostly determined by the value of ρ_c. From Figure 6, the effective gap is largest at the lowest density. The extreme superfluid models, of course, give much more quenching of the emissivity, again with the quenching being greater at smaller ρ_c.

In summary, the observation of an intermediate value of the surface temperature of a neutron star would be evidence for both rapid cooling and superfluid quenching. Nevertheless, even if one knew the central density of the neutron star, the uncertain dependence of the gap energy on density would prevent a reliable estimate of the superfluid's maximum critical temperature.

3. ANALYTICAL MODEL

To understand the results of the numerical simulations, a qualitative explanation of the main trends is useful. In this section, we explore analytic solutions to the problem of neutron star cooling based on the schematic model of Figure 1, in which the heat stored in the crustal reservoir diffuses to the inner core where it is rapidly radiated by neutrinos. Energy transport in a neutron star is dominated by electron conduction, except in the outer envelope layers which can be treated separately. For clarity, we will initially ignore the effects of general relativity on the energy transport, but will include these effects in the final results. Such effects are included in the numerical calculations presented in § 2.

The Newtonian equations of radiative transport and energy balance are

$$L = -4\pi r^2 K \frac{\partial T}{\partial r}, \quad \frac{\partial L}{\partial r} = -4\pi r^2 C_V \frac{\partial T}{\partial t}, \tag{7}$$

where L is the luminosity and r is the radial coordinate. It is assumed that the structure of the neutron star does not change as the star cools. The thermal conductivity is K and the heat capacity is C_V. We apply these equations to the crust, where energy losses via neutrino emission serve primarily to determine the initial temperature profile but are unimportant compared with conduction in the presence of the temperature inversion.

The thermal conductivity K in our numerical simulations, in the solid phase, is taken from Itoh et al. (1984) and, in the liquid regime, is taken from Itoh et al. (1983) (with quantum corrections from Mitake, Ichimaru, & Itoh 1984). These conductivities are functions of the nuclear abundance and the charge and mass of the nuclei, which, in turn, have been estimated using the LLPR (Lattimer et al. 1985) EOS. The resulting conductivity is shown in Figure 8 as a function of density and temperature for matter below nuclear density. It is

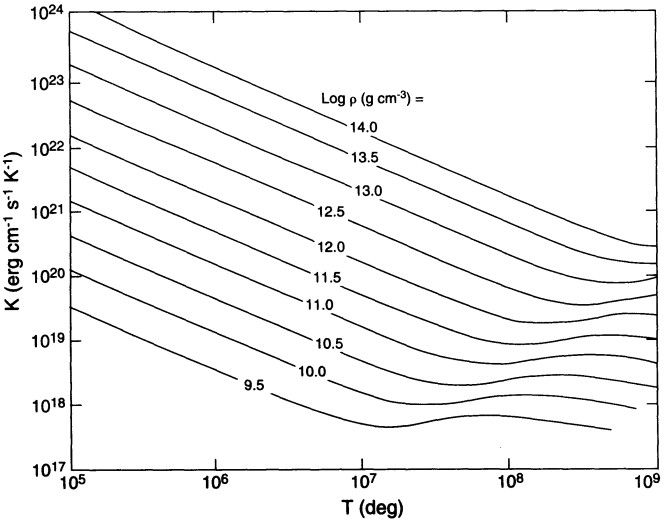

FIG. 8.—Thermal conductivity of neutron star matter

apprent that for temperatures below several times 10^7 K the conductivity varies as $1/T$, but above 10^8 K the conductivity is nearly independent of T. For the purposes of this section, we choose to parameterize K to reflect each of these dependencies as

$$K \simeq \frac{A_m}{T^m}\left(\frac{\rho}{\rho_0}\right)^s, \tag{8}$$

where, for $m = 1$, $A_1 \simeq 4 \times 10^{29}$ ergs K cm^{-1} s^{-1} and $s = 1$ and, for $m = 0$, $A_0 \simeq 10^{21}$ ergs cm^{-1} s^{-1} and $s = \frac{2}{3}$.

The specific heat is dominated by the degenerate nucleons at densities above the neutron drip density, 4×10^{11} g cm^{-3}. Additional contributions from the relativistic, degenerate electrons and from the ions are relatively small above the neutron drip density. The electron contributions become important if the matter contains superfluid neutrons. The details of the specific heat depend on the composition of the matter. The specific heat employed in the numerical simulations is shown in Figure 9 and was calculated using the composition from the LLPR

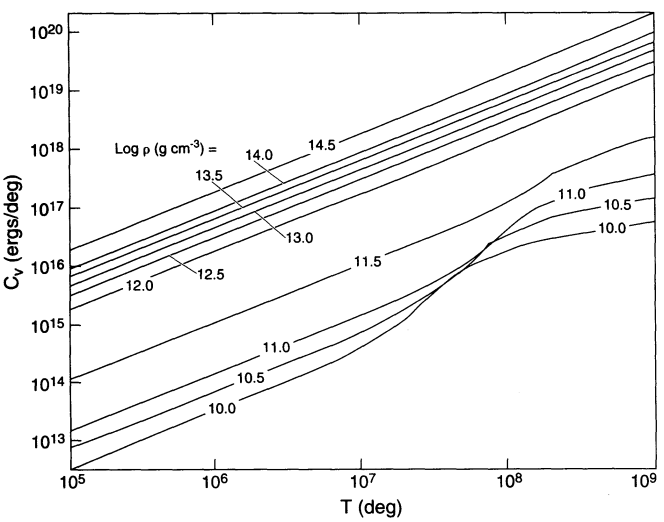

FIG. 9.—Specific heat of normal neutron star matter. The structure at high T and low ρ is due to ion contributions.

(Lattimer et al. 1985) EOS. It is evident that the specific heat above 10^{12} g cm^{-3} can be well approximated by

$$C_V \simeq B\left(\frac{\rho}{\rho_0}\right)^{1/3} T\,, \tag{9}$$

where $B \simeq 1.6 \times 10^{11}$ ergs K^{-2} cm^{-3}.

In general, the density varies rapidly with depth in a neutron star. In the outermost layers, where relativistic electrons dominate the EOS, $P \propto \rho^{4/3}$. In these regions, hydrostatic equilibrium dictates that $\rho(r) \propto (R-r)^3$, where $R-r$ is the depth. Beyond the neutron drip density, this relation changes. In the bulk of the crust, we have found that $\rho \propto (R-r)^n$, where $n \simeq 8$. At and above nuclear densities, in the core, the density dependence becomes much less steep.

Combining equations (7)–(9), one may derive the diffusion equation governing transport in the crust of a neutron star:

$$\frac{1}{r^2}\frac{\partial}{\partial r}\left[\frac{A_m}{T^m}\left(\frac{\rho}{\rho_0}\right)^s r^2 \frac{\partial T}{\partial r}\right] = B\left(\frac{\rho}{\rho_0}\right)^{1/3} T\,\frac{\partial T}{\partial t}\,. \tag{10}$$

We will treat separately the two forms of the thermal conductivity, labeling the cases with the power m.

Figure 3 shows the detailed internal thermal evolution for one of the models described in § 2. Although the temperature profile in the crust ($\rho < 2 \times 10^{14}$ g cm^{-3}, or $r > 9.1$ km) is not initially flat, by the time the cooling wave begins to propagate, the profile has flattened appreciably. Thus, for an initial condition, we may assume that the temperature is constant throughout the neutron star crust. The core cools rapidly and within hours becomes isothermal, with a temperature that is well below that of the crust. In this case, there is an inner boundary condition describing the core-crust interface temperature as a function of time (Pizzochero 1991). If both the conductivity and specific heat were independent of temperature and density, analytic solutions of the partial differential equations could be found employing an arbitrary inner boundary condition. Indeed, in the limit that the crust is thin, Pizzochero (1991) has found solutions for this case. However, in general, the conductivity and specific heat are temperature dependent, and an analytic solution of the general diffusion equations is not possible. Instead, we choose to simplify the initial and boundary conditions so that separable time and radial solutions can be found even if C_V and K are functions of T.

Let

$$T = T_0\,\psi(r)\phi(t)\,, \tag{11}$$

where T_0 is the initial temperature at the crust-envelope interface [i.e., $T_0 = T_m(t=0)$, and $\phi(0) = 1$]. We also define the dimensionless depth $x = (R-r)/R_{\rm shell}$, where $R_{\rm shell} = R - R_{\rm core}$, and the inverse of the relative crustal shell thickness, $q = R/R_{\rm shell}$. Assuming that $\rho_{\rm core} = \rho_0$, and using the density law $\rho = \rho_0 x^n$, we find

$$\frac{x^{-n/3}}{\psi^2}\left[\frac{d}{dx}\frac{x^{ns}}{\psi^m}\frac{d\psi}{dx} - \frac{2x^{ns}}{\psi^m(q-x)}\frac{d\psi}{dx}\right] = \frac{B}{A_m} R_{\rm shell}^2\, T_0^{1+m}\phi^m \frac{d\phi}{dt} = -\alpha\,, \tag{12}$$

where α is a separation constant. The function ψ is chosen to satisfy, at the surface, $\psi(0) = 1$ and $\psi'(0) = 0$. At the core-crust boundary $\psi(1) = T_{\rm core}/T_0 \sim \frac{1}{30}$. Note that $\psi(1)$ is the ratio of the core and crust temperatures. The value $\frac{1}{30}$ can be gleaned from Figure 3 (for $t \sim 1$ yr), which is typical for cooling simulations in which superfluidity does not occur. In the presence of superfluidity, $\psi(1)$ is about 3 times larger. Note that our model requires that $\psi(1)$ remains constant with time, despite the fact that $\psi(1) \to 1$ when $t > t_w$ (see Fig. 3). Nevertheless, it will become apparent that the full numerical solutions give results similar to those of the simplified model.

We immediately note from the right-hand side of equation (12) that the cooling time is predicted to be proportional to $R_{\rm shell}^2/D$, where the diffusivity $D \sim A/B$, just as Brown et al. (1988) surmised. This is to be compared to the numerical simulations displayed in Figure 4, in which $t_w \propto R_{\rm shell}^n$, where $1.7 \lesssim n \lesssim 1.8$. The deviation is explained below.

The time dependence is elementary for the two cases of m:

$$\begin{aligned} m = 1:\quad & \phi = \sqrt{1 - \frac{t}{\tau}}\,, \\ & \tau = \frac{BT_0^2}{2A_1\alpha} R_{\rm shell}^2 \simeq 67 T_{9,0}^2 \left(\frac{R_{\rm shell}}{\rm km}\right)^2 \alpha^{-1}\ {\rm yr}\ ; \\ m = 0:\quad & \phi = 1 - \frac{t}{\tau}\,, \\ & \tau = \frac{BT_0}{A_0\alpha} R_{\rm shell}^2 \simeq 53 T_{9,0} \left(\frac{R_{\rm shell}}{\rm km}\right)^2 \alpha^{-1}\ {\rm yr}\,. \end{aligned} \tag{13}$$

Above, we have used the notation $T_{9,0} = T_0/10^9$ K. Although the time dependencies we derived are oversimplified, it can still be argued that the time $t_w \sim \tau$. The precise value of the cooling time still depends on α, which must be determined from the solution of the radial equation.

To find analytic solutions to the radial equation, further simplifications must be taken. We will assume that the density is constant in the crust, i.e., $n = 0$. Consider, for the moment, the case in which the crust thickness is relatively small, i.e., $q \to \infty$. The radial equation becomes

$$\frac{1}{\psi^2}\frac{d}{dx}\frac{1}{\psi^m}\frac{d\psi}{dx} = -\alpha\,. \tag{14}$$

If $m = 1$, we find the analytic solution,

$$\psi = \frac{1}{\cosh(\sqrt{\alpha}x)}\,, \tag{15}$$

where

$$\alpha = [\cosh^{-1}\psi(1)^{-1}]^2 \simeq 17\,. \tag{16}$$

In the case $m = 0$, the solution can be expressed as a power series:

$$\psi = \sum_{n=0}^{\infty} a_n \alpha^n x^{2n}\,, \tag{17}$$

with the constraints that $\psi(0) = a_0 = 1$ and $\psi'(0) = 0$. The first few a_n are $a_1 = -1/2$, $a_2 = 1/12$, $a_3 = -1/72$, $a_4 = 1/524$, etc. The separation constant satisfies $\sum a_n \alpha^n = \psi(1)$, which yields $\alpha \simeq 3$ in the limit $\psi(1) \to 0$. Thus, assuming fiducial values of $T_0 = 10^9$ K (see Fig. 3) and $R_{\rm shell} = 1$ km, the cooling time is about 4 yr for the case $m = 1$. For the case $m = 0$ the cooling time is about 17 yr. The latter value is surprisingly close to those deduced from Figure 4, namely about 15 yr in the absence of superfluidity in the crust (if $T_{9,0} = 1$).

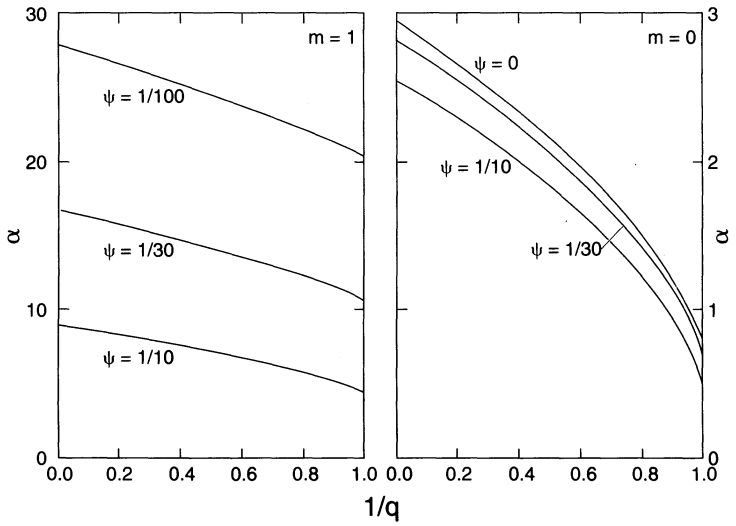

FIG. 10.—Separation constant α as a function of $\psi[\equiv\psi(1)]$ and q. The left-hand panel is for the case $m = 1$; the right-hand panel is for the case $m = 0$.

In more general cases, the separation constant α depends also on q, $\psi(1)$ and n. These relations are shown in Figure 10 for $n = 0$. Clearly, as long as $q > 0.5$, i.e., as long as the shell is less than 50% of the star's radius, the separation constant is relatively insensitive to q. Note that α decreases, i.e., the cooling time increases, as the star's crust occupies a larger and larger fraction of the star. In the numerical results shown in Figure 4, this behavior is visible as the positive curvature in the $R_{\rm shell}$ curves.

The quantity α also depends upon the value of $\psi(1)$. In the case $m = 0$, this dependence is rather small. In the case $m = 1$, the dependence is larger and will affect the calibration of the $t_w - R_{\rm shell}$ theoretical relation. In addition, the full solution of equation (12) is sensitive to the power, n, of the radial dependence of the density. In general, for values of $n > 1$, no reasonable solutions satisfying the boundary conditions we selected are possible. The assumption that separable time and radial solutions exist is incompatible with a strong density dependence. To proceed further with less drastic approximations is tantamount to solving the general transport equations. However, the chief aim in this section is to provide analytic support for the full numerical results. Inasmuch as the numerical results quantitatively agree with the $n = 0$ models, our basic aim is achieved.

We have observed that the numerical simulations shown in Figure 4 have a slope of about 1.7–1.8, while the analytic solutions predict a slope of 2. This difference is due to the neglect of general relativity in the analytic solution. It is straightforward to include the general relativistic modifications in the case of a thin shell, i.e., equation (13). Assuming that the star's structure is static, and that the metric functions do not vary within the star's crust, one finds

$$\tau = \frac{BT_0^{1+m}}{(1+m)A_m\alpha} R_{\rm shell}^2 \Gamma^3 , \qquad (18)$$

where $\Gamma = 1/\sqrt{1 - 2GM/Rc^2}$. In Figure 11, we have replotted the cooling simulations discussed in § 2 using $R_{\rm shell}^2\Gamma^3$ as the abcissa. Two cases are shown, depending upon the precise definition of $\rho_{\rm core}$ and, thus, $R_{\rm shell}$. The scatter of the data is reduced and the slope of the resulting best fits becomes nearly equal to 1. In the case $\rho_{\rm core} = \rho_0$, the best-fit slopes are 1.00 (0.91) for the nonsuperfluid (superfluid) crust situations. In the case $\rho_{\rm core} = 0.5\rho_0$, the best-fit slopes are 1.09 (1.01) for the nonsuperfluid (superfluid) crust situations. In the case $\rho_{\rm core} = \rho_0$, there is a small positive curvature due to the variation of α with $R_{\rm shell}/R$, but this is not apparent in the other case since $R_{\rm shell}$ is less.

Thus, equation (18) seems to be an accurate description of the relationship between the cooling time and the structure. Although numerical factors can be estimated from values for A, B, and T_0, it is simpler and more accurate to calibrate this relation from the numerical simulations. This calibration will depend upon the definition of $\rho_{\rm core}$. Combining the results of all the numerical simulations reported in § 2 for superfluid crusts (SF), we obtain

$$t_w \simeq \begin{cases} 8.4 \pm 2.0(R_{\rm shell}/1\ {\rm km})^2(1 - 2GM/Rc^2)^{-3/2}\ {\rm yr}\ , \\ 2.4 \pm 0.25(R_{\rm shell}/1\ {\rm km})^2(1 - 2GM/Rc^2)^{-3/2}\ {\rm yr}\ , \end{cases} \qquad (19)$$

where the first case is for $\rho_{\rm core} = 0.5\rho_0$ and the second refers to $\rho_{\rm core} = 1.0\rho_0$. For the nonsuperfluid cases, the average cooling time is about a factor of 3.5 times larger than given by equation (19). Note that the accuracy of equation (19) is sensitive to the definition of $\rho_{\rm core}$. The fit becomes more accurate as the definition of the crust is broadened, presumably because the region between $0.5\rho_0$ and ρ_0 contributes substantially to the resistance to heat flow through the crust.

Given the large range of masses and equations of state for which we have calculated cooling times, it is significant that the results can be fitted to such a simple formula as equation (19). In addition, we have verified that this relationship is valid for EOSs that contain extensive phase transitions, such as those for kaon condensates and quark matter discussed in Thorssen et al. (1994). If $R_{\rm shell}$ can be connected in a straightforward way to M and R, observations of the rapid surface cooling of a young neutron star can yield important information concerning the structure of the star. We explore this connection in the next section.

4. NEUTRON STAR STRUCTURE

Given a determination of t_w, what can be learned about the neutron star and/or the EOS? To analyze this, we examine the functional dependence of $R_{\rm shell}$ on the neutron star's mass and

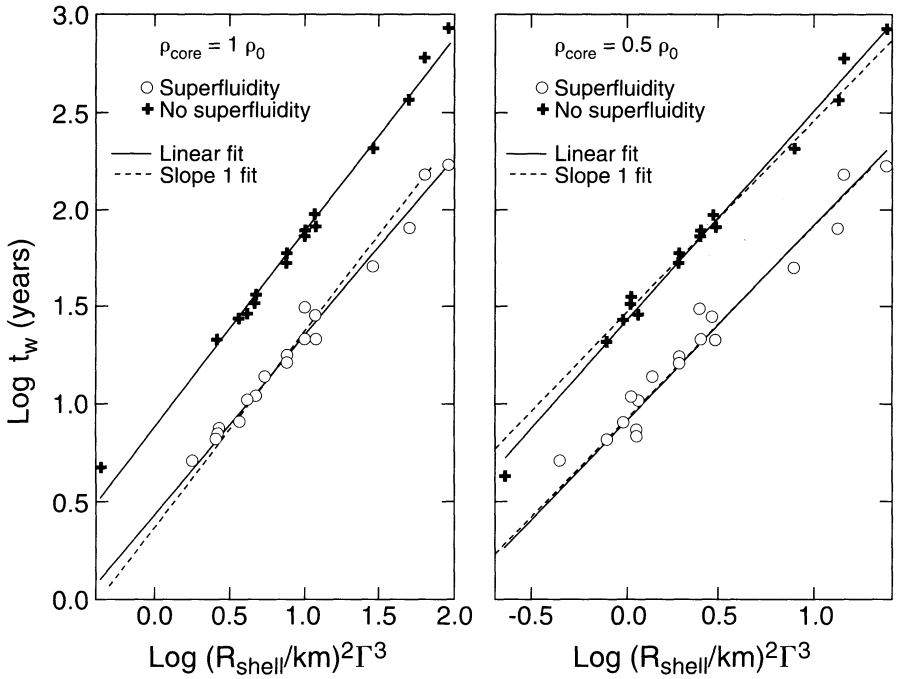

FIG. 11.—Neutron star cooling times. The points represent results of numerical simulations reported in § 2. The solid lines are the best-fit lines through the points; the dashed lines are the best-fits if the slope is assumed to be 1. The left-hand panel is for the case when R_{shell} is defined by $\rho_{core} = \rho_0$; the right-hand panel is for $\rho_{core} = 0.5\rho_0$.

radius. This function is not further dependent on the EOS at high density, including the existence or nonexistence of phase transitions. To see this, consider the relativistic equation of hydrostatic equilibrium:

$$\frac{dP}{dr} = -\frac{G[M(r) + 4\pi r^3 P/c^2](P/c^2 + \rho)}{r^2 - 2GM(r)r/c^2}, \qquad (20)$$

where $M(r) = \int 4\pi\rho r^2\, dr$ is the mass enclosed within radius r. We will apply this equation to the region between R_{core} and R, a region in which we can approximate $M(r) \simeq M$, where M and R are the total mass and radius. We can also neglect P/c^2 and the internal energy density relative to the mass density and $4\pi r^3 P/c^2$ relative to M. Hence, we will use the baryon density n instead of the mass density ρ. Equation (20) can then be integrated to yield

$$\mathscr{H} \equiv \int_0^{P_{core}} \frac{dP}{nmc^2} \simeq \frac{1}{2}\log\left(\frac{1 - R_s/R}{1 - R_s/R_{core}}\right), \qquad (21)$$

where $R_s = 2GM/c^2$. Here, P_{core} is the pressure at the core-crust interface, where the baryon density is n_{core}. The dimensionless quantity $\mathscr{H}$, at constant temperature and for matter in β equilibrium, is just μ_n/mc^2, where μ_n is the neutron chemical potential and m is the baryon mass. It is a function of the EOS at and below the density n_{core}. For instance, if the pressure below n_{core} varies with density in a polytropic fashion ($P \propto n^\gamma$), one obtains $\mathscr{H} = [\gamma/(\gamma - 1)](P_{core}/n_{core})$. Below nuclear density, γ is a complicated function of density because of phase transitions from nuclei to deformed nuclei and bulk matter (Lattimer et al. 1985). Though it is not possible to write a simple relation between $\mathscr{H}$ and P_{core}, the two are intimately connected via the EOS. But the most important result is that $\mathscr{H}$ is quite insensitive to uncertainties in the EOS above nuclear density.

Despite the fact that it depends only upon the EOS at and below nuclear density, values of $\mathscr{H}$ have a surprisingly large variation in the literature. Values of $\mathscr{H}$ for the equations of state we have used are listed in Table 4. However, it should be pointed out that the Pandharipande & Smith (1975) EOS is an extreme case (it does not include β equilibrium and it contains a neutron solid) and is not considered realistic. Neglecting this EOS, one sees that at the density n_0, variations in $\mathscr{H}$ amount to about a factor of 1.7 but are only about a factor of 1.04 at the density $0.5n_0$.

The reason for the large uncertainty near n_0 rests with the symmetry energy and incompressibility of nuclear matter.

TABLE 4

VALUES OF $\mathscr{H} = \int_0^{P_{core}} dP/nmc^2$

EOS	$\mathscr{H}(n_{core} = 0.5n_0)$	$\mathscr{H}(n_{core} = n_0)$
Bethe, Pethick, & Sutherland 1971	0.0248	0.0334
Friedmann & Pandharipande 1981	0.0248	0.0402
Pandharipande & Smith 1975	0.0415	0.0965
Prakash, Ainsworth, & Lattimer 1988[a]	0.0259	0.0568

[a] $S_0 = 30$ MeV; $F(u) = u$; Negele & Vautherin 1980 assumed for $n < 0.5n_0$.

These dependencies are easy to see. In the standard way, one may write the energy per baryon of cold nuclear matter as an expansion:

$$E(u, x) = E(u, \tfrac{1}{2}) + S(u)(1 - 2x)^2 + \cdots , \quad (22)$$

where $u = n/n_0$ is the normalized baryon density. In equation (22), $E(u, \frac{1}{2})$ is the energy per baryon of symmetric matter, x is the proton fraction, and $S(u)$ is the (density-dependent) symmetry energy [note that $S_0 \equiv S(1)$]. It has been argued (see, e.g., PAL) that this expression is adequate for all values of x, including $x = 0$ (neutron matter). The total energy is obtained by adding the specific lepton energy $E_L(u, x)$, and in β equilibrium, one has $\partial(E + E_L)/\partial x = 0$. The equilibrium proton fraction at $u = 1$ is small: for the plausible range 25 MeV $\leq S_0 \leq 35$ MeV, one has $0.024 \leq x \leq 0.054$. For small proton fractions in the vicinity of $u = 1$, the pressure-to-density ratio is

$$\frac{P(u)}{un_0} \simeq \frac{K_0}{9}(u - 1) + u\frac{\partial S(u)}{\partial u} , \quad (23)$$

where K_0 is the incompressibility parameter. At $u = 1$, this depends only on S. In addition to the uncertainty in S_0, there is also considerable disagreement regarding the density dependence of S. Moreover, at lower densities there will be contributions from the incompressibility term, which differ among these equations of state. Below the density $0.5n_0$, however, nuclei are present, there are fewer free nucleons around, and the pressure is dominated by electrons, and the EOS of nuclear matter plays a secondary role in determining the pressure.

Because the value of $\mathscr{H}$ becomes progressively more uncertain at higher densities, it is advantageous to set $n_{\rm core}$ to a value less than n_0. This is opposite to the trend noted in equation (19), in which the derived relationship between t_w and $R_{\rm shell}$ was found to be more accurate for larger values of $n_{\rm core}$. Nevertheless, for the case $n_{\rm core} = 0.5n_0$, the gain in accuracy in $\mathscr{H}$ is larger than the loss of accuracy in equation (19).

Combining equations (19) and (21), we can establish limits to M and R for a given value of t_w, should one ever be observed. For the case of superfluidity in the crust, these limits are shown in Figure 12. This figure shows how an observed value of t_w could confine a neutron star's position in a mass-radius diagram. Even though the estimated error of the fit given in equation (19) is of order 25%, the limits are interestingly tight. Useful information can be obtained even if the mass of the neutron star cannot be independently determined. Theoretical arguments suggest that neutron stars produced in gravitational collapse supernovae are in the range $1.15\ M_\odot \lesssim M \lesssim 1.5\ M_\odot$. The estimated masses of 10 neutron stars measured by using radio pulsars in binary systems (e.g., Thorsett et al. 1993) are consistent with this range. Thus, if $t_w = 10$ yr, this theoretical mass range implies a radius range of 9 km $\lesssim R \lesssim$ 11.5 km if the crust is superfluid and a range of 6.8 km $\lesssim R \lesssim$ 8.5 km if the crust is nonsuperfluid. Because of the restricted radius range, the nature of the high-density EOS would itself be constrained by this result. Although further work on the EOS and the nature of superfluidity at subnuclear densities may modify the regions illustrated in Figure 12, the qualitative relationship between rapid cooling and structure will remain unaltered.

5. CONCLUSIONS

We have considered the implications of neutron stars cooling very rapidly compared to the standard case, in which cooling is via modified Urca processes. Such stars will undergo a sharp decrease in surface temperature at the time t_w, which is essentially given by the thermal diffusion time through the

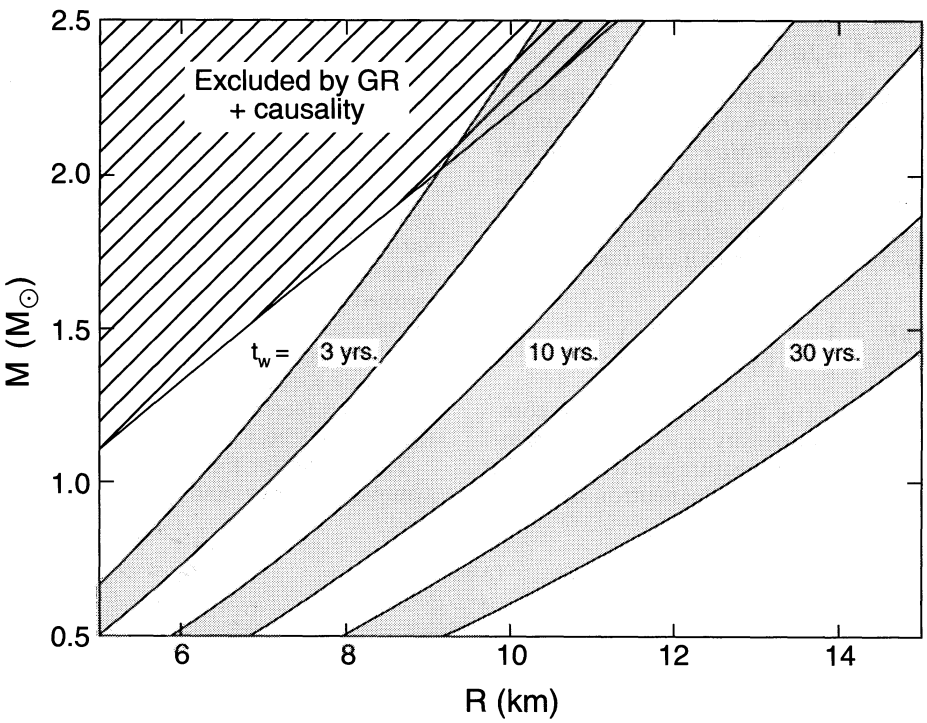

FIG. 12.—Shaded areas are the allowed regions of mass and radius for a neutron star observed to have the indicated values of the rapid cooling time t_w. It is assumed that $\rho_{\rm core} = 0.5\rho_0$ and that the neutron star crust is superfluid. The mass-radius region excluded by general relativity and causality is indicated by the hatched region.

crust. This time primarily depends on the square of the thickness of the crust but is modified by relativistic effects and is also influenced by the presence of neutron superfluidity in the crust. The time is not very sensitive to the details of the accelerated emissivity, such as the density threshold or the net rate, including the question of whether or not superfluidity quenches the rapid cooling. The surface temperature during the isothermal phase following the time t_w, on the other hand, depends strongly on the details of the superfluid gaps above nuclear density and on the central density of the star, both of which are uncertain.

We have shown that the crustal thickness, appropriately defined, depends only on the mass and radius of a neutron star with a relatively small uncertainty arising from the EOS. An observational determination of t_w, and the subsequent inference of the crustal thickness, would therefore constrain the structure of the star. An estimate of the mass of the neutron star would, in addition, constrain the high-density EOS.

We gratefully acknowledge discussions with T. Ainsworth, D. Page, C. J. Pethick, and F. D. Swesty. We are especially indebted to A. D. Jackson for pointing out to us the solution equation (15). This research was supported in part by the Department of Energy under grants DE-FG02-87ER40317 and DE-FG02-88ER40388 and in part by the Laboratory Directed Research and Development program at the Los Alamos National Laboratory of the United States Department of Energy.

REFERENCES

Anderson, S. B., Córdova, F. A., Pavlov, G. G., Robinson, C. R., & Thompson, R. J., Jr. 1993, ApJ, 414, 867
Bailin, D., & Love, A. 1984, Phys. Rep., 107, 325
Baym, G., Pethick, C., & Sutherland, P. 1971, ApJ, 170, 299
Becker, W., Trümper, J., & Ögelman, H. 1993, in Isolated Pulsars, ed. K. A. Van Riper, R. Epstein, & C. Ho (Cambridge: Cambridge Univ. Press), 104
Brinkmann, W., & Ögelman, H. 1987, A&A, 182, 71
Brown, G. E., Kubodera, K., Page, D., & Pizzochero, P. 1988, Phys. Rev. D, 37, 2042
Burrows, A., & Lattimer, J. M. 1986, ApJ, 307, 186
Chao, N.-C., Clark, J. W., & Yang, C.-H. 1972, Nucl. Phys. A., 179, 320
Córdova, F. A., Hjellming, R. M., Mason, K. O., & Middleditch, J. 1989, ApJ, 345, 451
Finley, J. P., Ögelman, H., & Kızıloğlu, Ü. 1992, ApJ, 394, L21
Friedman, B., & Pandharipande, V. R. 1981, Nucl. Phys. A, 361, 502
Gorenstein, P., Seward, F., & Tucker, W. 1983, in Supernova Remnants and Their X-Ray Emission, ed. J. Danziger & P. Gorenstein (Dordrecht: Reidel), 1
Halpern, J. P., & Holt, S. S. 1992, Nature, 357, 222
Helfand, D. J., Chanan, G. A., & Novick, R. 1980, Nature, 283, 337
Hoshi, R. 1992, in The Structure and Evolution of Neutron Stars, ed. D. Pines, R. Tamagaki, & S. Tsuruta (New York: Addison-Wesley), 98
Inoue, H. 1992, in The Structure and Evolution of Neutron Stars, ed. D. Pines, R. Tamagaki, & S. Tsuruta (New York: Addison-Wesley), 63
Itoh, N., Kohyama, Y., Matsumoto, N., & Seki, M. 1984, ApJ, 285, 758
Itoh, N., Mitake, S., Iyetomi, H., & Ichimaru, S. 1983, ApJ, 273, 774
Kiguchi, M., & Sato, K. 1981, Prog. Theor. Phys. Lett., 66, 725
Lattimer, J. M., Pethick, C. J., Prakash, M., & Haensel, P. 1991, Phys. Rev. Lett., 66, 2701
Lattimer, J. M., Pethick, C. J., Ravenhall, D. G., & Lamb, D. Q. 1985, Nucl. Phys. A., 432, 646
Lattimer, J. M., & Yahil, A. 1989, ApJ, 340, 426
Levenfish, K. P., & Yakovlev, D. G. 1993, in The Physics of Strongly Coupled Plasma, ed. H. M. Van Horn & S. Ichimaru (Rochester: Univ. of Rochester Press)
Lorenz, C. P., Ravenhall, D. G., & Pethick, C. J. 1993, Phys. Rev. Lett., 70, 379
Maxwell, O. V., Brown, G. E., Campbell, D. K., Dashen, R. F., & Manassah, J. T. 1977, ApJ, 216, 77
Miralles, J., & Van Riper, K. A. 1993, in preparation
Mitake, S., Ichimaru, S., & Itoh, N. 1984, ApJ, 277, 375
Negele, J. W., & Vautherin, D. 1973, Nucl. Phys. A, 207, 298
Ögelman, H. 1993, in Isolated Pulsars, ed. K. A. Van Riper, R. Epstein, & C. Ho (Cambridge: Cambridge Univ. Press), 96
Pandharipande, V. R., & Smith, R. A. 1975, Nucl. Phys. A, 237, 507
Page, D., & Applegate, J. H. 1992, ApJ, 394, L17
Pizzochero, P. 1991, Phys. Rev. Lett., 66, 2425
Prakash, M., Ainsworth, T. L., & Lattimer, J. M. 1988, Phys. Rev. Lett., 61, 2518
Prakash, M., Prakash, M., Lattimer, J. M., & Pethick, C. J. 1992, ApJ, 390, L77
Pye, J. P., Pounds, K. A., Rolf, D. P., Seward, F. D., Smith, A., & Willingale, R. 1981, MNRAS, 194, 569
Takatsuka, T. 1972, Progr. Theor. Phys., 48, 1517
Thorsett, S. E., Arzoumanian, Z., McKinnon, M. M., & Taylor, J. H. 1993, ApJ, 405, L29
Thorssen, V., Prakash, M., & Lattimer, J. M. 1994, Nucl. Phys. A, in press
Tsuruta, S. 1986, Comm. Astrophys., 1, 151
Van Riper, K. A. 1988, ApJ, 329, 339
———. 1991, ApJ, 75, 449